

Pressure-Induced Foaming of Metals

FRANCISCO GARCÍA-MORENO,^{1,2,4} MANAS MUKHERJEE,³
CATALINA JIMÉNEZ,¹ and JOHN BANHART^{1,2}

1.—Helmholtz-Centre Berlin for Materials and Energy, 14109 Berlin, Germany. 2.—Technical University Berlin, 10623 Berlin, Germany. 3.—Indian Institute of Technology, Madras, Chennai 600 036, India. 4.—e-mail: garcia-moreno@helmholtz-berlin.de

Pressure-induced foaming (PIF) of metals is a foaming technique in which blowing agent free compacted metal powders are foamed. The method consists of heating hot-compacted metallic precursors to above their melting temperature under gas overpressure and foaming them by pressure release. This study focuses on PIF of Al99.7 and AlSi7 alloys under both air or Ar and overpressures up to 9 bar. In situ x-ray radiography allows us to follow the foaming process and to perform quantitative analyses of expansion, foam morphology, and coalescence rate. Mass spectrometry helps to identify hydrogen as the foaming gas. Adsorbates on the former powder particles are found to be the primary gas source. Various advantages of this new method are identified and discussed.

INTRODUCTION

The powder metallurgical (PM) foaming route for producing metallic foams has already found industrial application.¹ Metallic foam blocks,² sandwich panels,^{3,4} or foams with more complex geometries are manufactured through special variants of the process.^{5,6} Commonly, a chemical blowing agent is admixed to a mixture of metal powders, after which the blend is hot pressed to a foamable precursor, whose foaming is induced by heating to above the melting temperature of the alloy and the decomposition temperature of the blowing agent. TiH₂ is the most frequently used blowing agent for aluminum alloys.

One disadvantage of this method, besides the high cost of the blowing agent, is the still insufficiently uniform pore structure of the resulting foam. Structural heterogeneities start to form during pore nucleation, which is accompanied by the accumulation of gas at residual pores in the vicinity of blowing agent or alloying element particles.^{7–9} The reasons for such heterogeneities include the broad particle size distribution of the blowing agent, the nonlinear temperature dependence of gas release, and spatial gradients of foaming associated with the unavoidable temperature distribution in the sample.^{10,11} Furthermore, the heating rate and ambient atmosphere also have a crucial influence on foaming.^{12–14} Many attempts to optimize the gas pro-

duction kinetics have been made, e.g., by using different blowing agents such as ZrH₂, CaCO₃, MgH₂, etc.,¹¹ using mixtures of agents,¹⁵ varying the amount of blowing agent,¹² or engineering a precise heating profile.¹⁴ Another approach is to preheat the TiH₂ in the presence of oxygen, thus creating a protective oxide layer that serves as a diffusion barrier, retarding the kinetics of the gas decomposition and thereby shifting the onset temperature of hydrogen release toward the melting temperature of the alloy used.^{10,16–19}

The heterogeneities may further grow during foam expansion, caused, e.g., by temperature gradients, pore coalescence, coarsening, etc. Further defects can even develop during solidification.²⁰ The undesirable consequence of having a few large pores is that they induce a lower local density region that is weaker upon mechanical deformation.²¹

A new approach to avoid all the difficulties associated with blowing agents is to produce foams without them. One method to foam Mg alloys without blowing agent was presented by Renger and Kaufmann.²² They create a vacuum to expand the gas contained in slurries that had been melted under normal pressure and produce Mg foam. By this method, the gas contained in the slurries and trapped in the melt is sufficient for foaming if the outer pressure is reduced. The hydrogen solubility in aluminum and Al alloy melts, however, is much lower than in Mg-based melts.²³ Furthermore,

oxides ensure Mg foam stabilization. Normal Mg melts contain 1–2% of such oxides²⁴ and even more after adding Mg slurries.²² The oxide content in usual Al powders is only 0.3–0.7%,^{25–27} and this seems not to be enough for foam stabilization. Therefore, in its current form, the method from Renger cannot be used to foam Al-based alloys. Another method to foam Al and Al alloys was introduced by the authors.²⁸ Again a vacuum allows to expand a cast melt using the dissolved hydrogen as foaming gas, but in this case, foam nucleation, expansion, and solidification occur in a few seconds, which allows to obtain a sufficiently stable foam structure although only a reduced amount of stabilizing oxides is present.

Pressure-induced foaming (PIF) does not require any additional gas-releasing agent,^{29,30} and it is applicable to the production of Al-, Zn-, or Mg-based foams. It relies on the fact that the gas contained in a powder sample compacted under normal atmospheric pressure is sufficient for foaming. Therefore, it is important to hold as much of this gas as possible inside the precursor until the whole precursor is melted. Foam stabilization is provided by the oxides contained in the powders as for the standard PM route. Good consolidation of the metal powder is required to provide a *gas-tight* precursor. For this, the precursor has to reach high densities and exhibit metallic bonding between the powder particles.

In the following, the PIF method is described in detail, as well as its advantages for foaming. In situ x-ray radiography is applied to a series of Al99.7 and AlSi7 samples that are foamed under different atmospheres and overpressures. In this article, we specially discuss in detail and quantitatively all possible gas sources contributing to foaming and their influence on foam formation.

EXPERIMENTAL METHODS

Precursor Preparation

Precursors of Al99.7 and AlSi7 (in wt.%) were prepared by uniaxial hot compaction after mixing the elemental powders. No blowing agents were added. Air-atomized aluminum powder from Alpoco ($D_{50} = 38 \mu\text{m}$, $D_{90} = 76 \mu\text{m}$, purity 99.7%; AMG Alpoco UK Ltd., Anglesley, U.K.) was used. Silicon powder ($D_{50} = 26 \mu\text{m}$, $D_{90} = 50 \mu\text{m}$) for alloying was procured from Wacker Chemie AG (Munich Germany). Reference samples containing TiH_2 from Chemetall GmbH (Frankfurt, Germany) with $D_{50} = 14 \mu\text{m}$ and $D_{90} = 34 \mu\text{m}$ were also manufactured. To prove the influence of gases adsorbed to the metal powder surfaces on foam expansion, Al powders were fractioned for certain experiments into different size classes by sieving, namely $<25 \mu\text{m}$, 25–40 μm , 40–50 μm , and 50–160 μm . A powder distribution analysis was performed with a Sympatec HELOS Vectra (Sympatec GmbH, Clausthal-Zellerfeld, Germany) laser particle

analyzer, and the mean particle sizes was measured to $D_{50} \approx 20 \mu\text{m}$, 32 μm , 47 μm , and 65 μm , respectively. The corresponding Brunauer, Emmett and Teller (BET Theory) surface area was obtained according to data sheets available in the literature.³¹

For standard precursor preparation (Al99.7 or AlSi7), 20 g of the corresponding powders was filled into a steel die of 36 mm diameter. The powders were first cold compacted under a uniaxial pressure of 300 MPa, after which they were heated to 400°C to be hot compacted for 5 min. Compaction was normally performed under normal atmosphere and pressure, although some samples were compacted under a reduced pressure of $\approx 10^{-2}$ bar as described elsewhere⁷ or at 2 bar Ar overpressure at otherwise identical conditions, in order to investigate the influence of gas entrapped in the precursor during compaction. Ar was used to minimize oxidation during compaction. Cold-compacted samples were produced for comparison to simulate the open porosity of nonsintered grains.

The density of the compacted samples was $99.4\% \pm 0.2\%$ of their theoretical density. From such tablets, sample precursors of volume $V_0 = 20 \times 10 \times 5 \text{ mm}^3 = 1 \text{ cm}^3$ were prepared for foaming.

Pressure-Induced Foaming

The x-ray-transparent pressure furnace used in this study consists of a sealed AlMg1 tube (outer diameter $\varnothing = 40 \text{ mm}$) with 0.5-mm wall thickness (see Fig. 1). On one end, electrical connections are led inside to a resistive ceramic heating plate (carbon layer embedded in Si_3N_4) and to thermocouples. On the other end, the gas inlet and outlet are fixed. The inlet tube is connected to a gas cylinder (or optionally to a vacuum pump), and the outlet line is connected to a pressure regulation valve. With this furnace, temperatures up to 700°C, heating rates up to 35 K/s, and pressures of 0.001 bar to 10 bar can be achieved as described elsewhere.³² Synthetic air, argon, or other gases can be used as cover gases and vacuum up to 10^{-3} bar can be achieved with a rotary pump.

Figure 2 shows the measured course of PIF of an AlSi7 sample, indicating the relative cross-sectional expansion $A_f(t)/A_0$, the temperature $T(t)$ and the schematic surrounding gas pressure profiles $p(t)$. PIF uses external gas overpressure—in this case $p_0 = 9 \text{ bar}$ —during the heating process of the powder compact until the sample has melted. After melting, the surrounding pressure is reduced to $p_1 = 1 \text{ bar}$, which triggers foaming immediately as the course of the projected area $A_f(t)/A_0$ in Fig. 2 shows. The time needed to release the pressure from p_0 to p_1 is defined as the foaming time t_f . A typical foaming time is $t_f = 25 \text{ s}$. For a few samples, different foaming times $t_f = 5 \text{ s}$, 25 s, and 60 s were applied. The waiting time t_w between melting and pressure release was in the range of $t_w = 10\text{--}100 \text{ s}$.

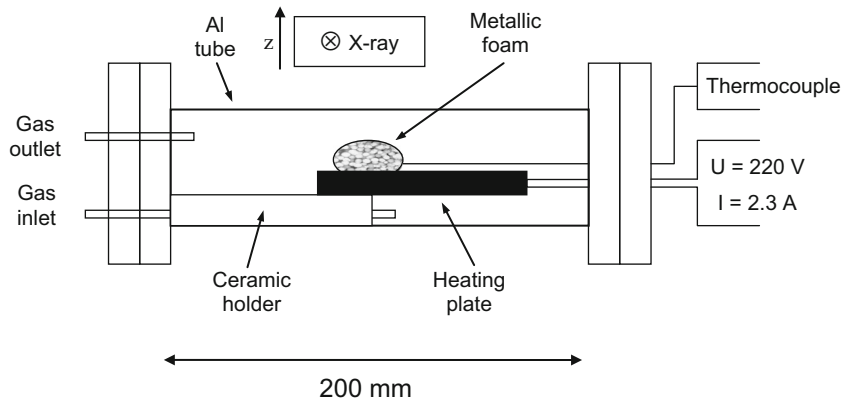


Fig. 1. Experimental setup of the furnace used to foam alloys and view them in situ by x-ray radioscropy. The x-ray transparent Al tube acting as a pressure foaming furnace is seen in the beam direction.

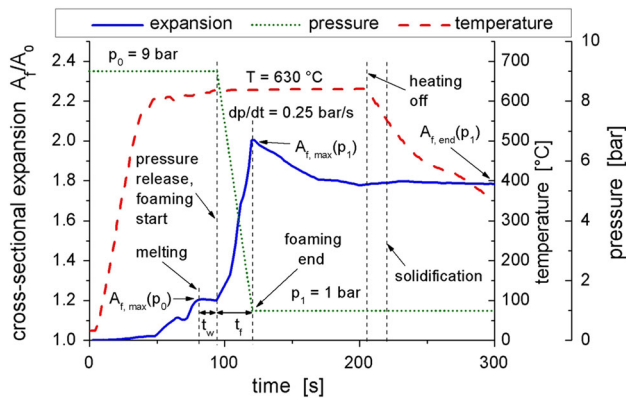


Fig. 2. Projected sample area expansion, sample temperature, and pressure in foaming chamber as a function of time for a AlSi7 sample compacted under normal atmosphere. $T_{end} = 630^{\circ}\text{C}$, $p_0 = 9$ bar, $p_1 = 1$ bar, $\Delta p/\Delta t = -0.25$ bar/s.

In Situ X-ray Analysis

X-ray radioscropy was performed with a radioscropy scanner comprising a 150 kV microfocuss tube L8121-01 and a flat panel detector C7942 (Hamamatsu, Tokyo, Japan), as described previously.³³ Series of high-resolution images (2240×2368 pixel) were acquired in situ, i.e., during melting, gas nucleation, and foaming, once per second. The self-developed radioscopic image analysis software AXIM (Analysis of X-ray Images) was used for automatic quantitative analysis of the foaming process from these images. This software allows us to calculate the relative cross-sectional expansion of the projected area of the foam $A_f(t)/A_0$, where $A_f(t)$ is the foam cross section and A_0 is the precursor cross section. The ratio $A_f(t)/A_0$ represents a two-dimensional expansion, which corresponds to the foam volume expansion $V_f(t)/V_0$ only when the foam is not allowed to expand in the direction of the x-ray beam. The uniaxially compacted precursors used in our experiments are known to expand anisotropically in the compaction direction in early foaming stages,³⁴ so that we can approximate

$$V_f(t)/V_0 \sim A_f(t)/A_0 \quad (1)$$

for the early stage, as the uniaxial compaction direction was oriented perpendicular to the beam. For later stages of foaming, however, we obtain nearly spherical foams, mostly possessing rotational symmetry around their vertical axis. In this case, we expect

$$V_f(t)/V_0 \sim (A_f(t)/A_0)^{3/2}. \quad (2)$$

In Situ Gas Release Analysis

Hydrogen evolution as a function of time and temperature is studied in a thermoanalyzer (409C; NETZSCH Pumps North America, LLC, Exton, PA) by mass spectrometry in an alumina tube furnace connected to a quadrupole mass spectrometer. The specific mass = 2 ion current represents the hydrogen release per sample mass unit. A total of 150 mg of Al powder compacts for two different powder sizes ($D_{50} \approx 20 \mu\text{m}$ and $65 \mu\text{m}$) were heated twice at 5 K/min from 40°C up to 750°C in flowing Ar atmosphere. Additionally, 150 mg of filings were prepared from powder compacts and heated under the same conditions.

RESULTS

General Expansion Behavior

PIF was successfully applied to Al99.7 and AlSi7 powder compacts in this work. No big difference in expansion or structure was found for AlSi7 compared to Al99.7. Also no notable differences in the foaming behavior were observed when using synthetic air or argon as cover gas. No marked influence of foaming time— $t_f = 5$ s, 25 s, and 60 s were tested—on the expansion behavior or pore size were found. In the first 90 s of heating an AlSi7 sample, we observed three initial expansion steps (see Fig. 2). The first is small, starts with heating, and is

related to thermal expansion. It corresponds to maximum $A_f(50\text{ s})/A_0 \approx 1.03$. The second takes place during gas nucleation $A_f(70\text{ s})/A_0 \approx 1.1$, whereas the third occurs after reaching the melting temperature of the alloy, at which the sample is completely melted and the maximal expansion under these pressure conditions is reached, namely $A_f(95\text{ s})/A_0 \approx 1.2$. In other words, at $p_0 = 9$ bar, the increase of the projected sample is just $\approx 20\%$. After releasing the pressure to $p_1 = 1$ bar, the foam expands in 25 s to $A_{f,\text{max}}(120\text{ s})/A_0 \approx 2$, i.e., $\approx 200\%$. During isobaric holding in the molten state for further 85 s up to $t = 205$ s, the foam shrinks continuously and reaches the end expansion of the solid foam of $A_{f,\text{end}}(300\text{ s})/A_0 \approx 1.8$ after heating is switched off.

Figure 3 shows x-ray images at different stages of the process and a cross section of the AlSi7 foam made by PIF, as described in Fig. 2. Round pores with diameters not exceeding 5 mm are observed. Furthermore, it was possible to demonstrate a considerable expansion in PIF-processed samples, even before pressure release (see Fig. 3b). The same experiment was performed for a bulk piece of cast Al99.7 that was molten under a gas pressure $p_0 = 9$ bar. As expected, the pressure release did not induce foaming. Similar behavior was found for Al99.7 and for AlSi7; therefore, further analysis was performed only for Al99.7.

Influence of Pressure

A series of Al99.7 foams was produced by first melting precursors under different Ar gas pressures— $p_0 = (1, 2, 4, 6, 9)$ bar—and then releasing pressure to $p_1 = 1$ bar. Foaming with different end pressures ($p_1 \neq 1$ bar), e.g., $p_0 = 9$ bar and $p_1 = 5$ bar (pressure drop $\Delta p = -4$ bar), was also

possible. However, with $p_0 = 1$ bar and $p_1 = 10^{-1}$ bar, large gas bubbles were obtained in the foam. These ruptured at the sample surface, and therefore the foam collapsed and degraded completely, similar to what was found previously for AlSi6Cu4.¹⁴ For $p_0 = 10^{-1}$ bar and $p_1 = 10^{-3}$ bar, only large gas bubbles appeared in the precursor already during melting and led again to bubble rupture at the sample surface, gas losses, and no foam. These observations indicate that evacuating a liquid Al foam from 1 bar leads to an unstable foam structure.²⁸ Therefore, an overpressure of around $p_0 > 1$ bar during melting is an essential requirement for foam expansion after pressure release for the type of powders used in this work. Other alloys or other oxide contents in the powders may lead to other critical p_0 .

The maximum expansion $A_{f,\text{max}}(p_0)/A_0$ after pressure release from p_0 to $p_1 = 1$ bar is given in Fig. 4 as a function of p_0 (full squares). A clear increase with increasing p_0 is found, although not as high as predicted from the ideal gas law (broken line) as will be discussed later. The expansion at the pressure release point $A_f(p_0)$ is also given in Fig. 4, showing a slight decrease with p_0 with a minimum at $p_0 = 4$ bar.

Applying an underpressure of $p_0 = 10^{-2}$ bar during heating of the precursor until complete melting, followed by a pressure increase up to $p_0 = 9$ bar and a subsequent pressure release to $p_1 = 1$ bar, did not give rise to foaming as will be discussed later.

Influence of Precursor Preparation

Figure 5 shows a foam made by applying typical PIF conditions ($T_{\text{end}} = 680^\circ\text{C}$, $p_0 = 5$ bar, $p_1 = 1$ bar,

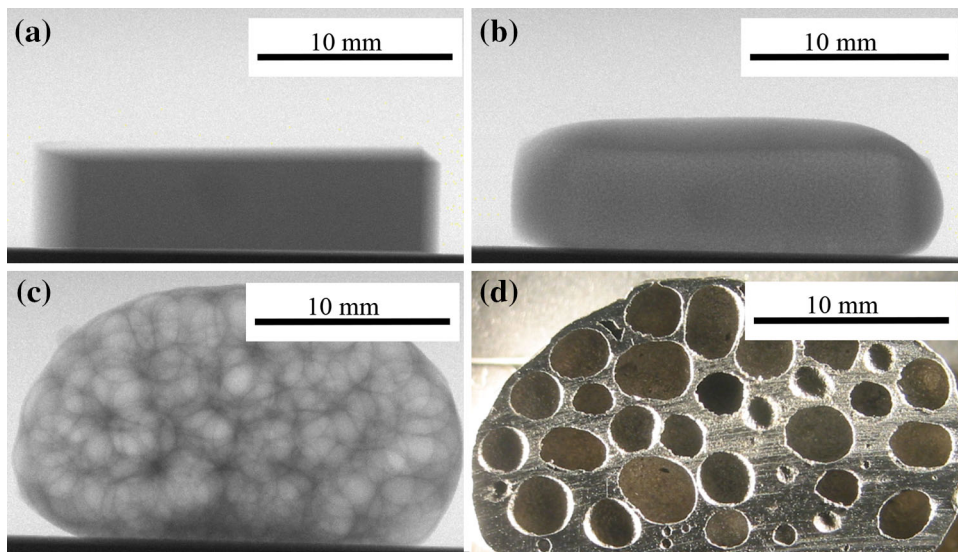


Fig. 3. X-ray images and cross section of an AlSi7 foam made by pressure induced foaming of a blowing-agent-free precursor compacted under normal atmosphere. $T_{\text{end}} = 630^\circ\text{C}$, $p_0 = 9$ bar, $p_1 = 1$ bar, $\Delta p/\Delta t = -0.25$ bar/s, $A_{f,\text{max}}/A_0 \approx 2$. (a) Precursor at $t = 1$ s, $p_0 = 9$ bar, $T = 25^\circ\text{C}$; (b) precursor containing nucleated gas bubbles at $t = 100$ s, $p_0 = 9$ bar, $T = 630^\circ\text{C}$; (c) expanded foam at $t = 125$ s after pressure release, $p_1 = 1$ bar, $T = 630^\circ\text{C}$; and (d) cross section of the solidified foam.

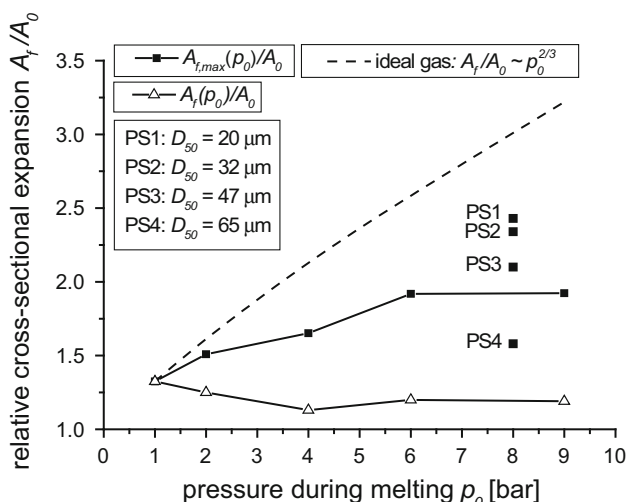


Fig. 4. Relative projected area $A_{r,max}(p_0)/A_0$ and $A_f(p_0)/A_0$ of Al99.7 foams after pressure release from p_0 to p_1 , $p_1 = 1$ bar, $\Delta p/\Delta t = -0.25$ bar/s, $T_{end} = 680^\circ\text{C}$ for as-received powder. PS(1-4): $A_{r,max}(p_0 = 8 \text{ bar})/A_0$ of precursors made from powders with different powder particle sizes ($D_{50} = 20, 32, 47,$ and $65 \mu\text{m}$) for $p_1 = 1$ bar. Data for as-received powder size taken from Ref. 29. The broken line represents the trend expected from the ideal gas law.

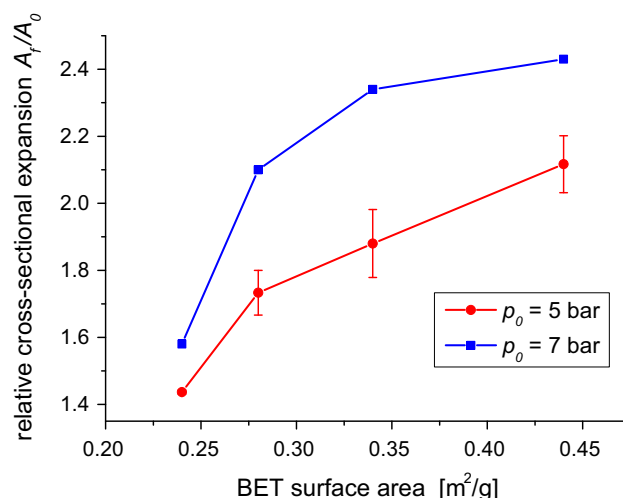


Fig. 6. Maximal expansion of Al foams made by PIF as a function of the BET surface area of the Al powder used for $p_0 = 5$ bar and 7 bar.

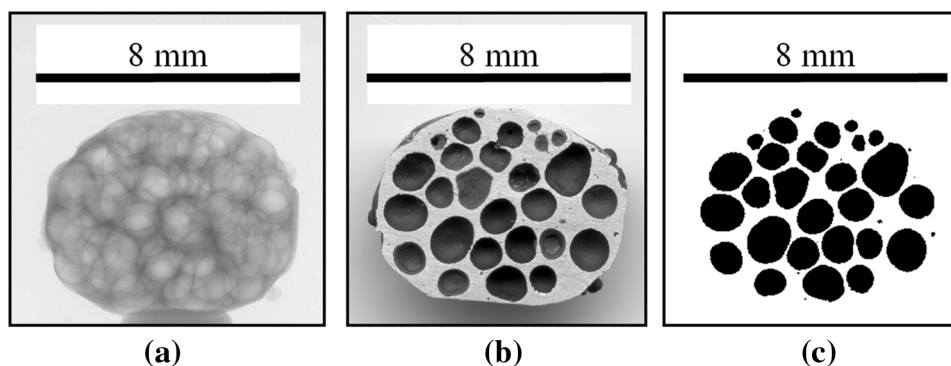


Fig. 5. (a) Radioscopy, (b) cross-section, and (c) binarized cross-sectional image of an Al foam made by PIF applying parameters $T_{end} = 680^\circ\text{C}$, $p_0 = 5$ bar, $p_1 = 1$ bar, $\Delta p/\Delta t = -0.16$ bar/s, $A_{max}/A_0 \approx 3$. Precursor was compacted under $\approx 10^{-2}$ bar pressure.

$\Delta p/\Delta t = -0.16$ bar/s) but from a precursor where powder was compacted under a pressure of $\approx 10^{-2}$ bar. Such precursors showed a better expansion and pore uniformity than when powder was compacted in air at 1 bar. An expansion of $A_{f,max}/A_0 \approx 3$ and homogeneous round pores were obtained. Precursors compacted under ≈ 2 bar Ar overpressure behaved like precursors compacted at 1 bar. In addition, samples made by cold-compacting powders were tested, to deliberately allow for some open porosity between the nonsintered grains. No foam was obtained in the last case.

Influence of Powder Particle Size

The surface area of the various sieved powders, which have different surface-to-volume ratios S_p/V_p , influences the maximum expansion of the

corresponding foams processed by PIF (see Fig. 6). Expansion markedly increases with decreasing particle size, i.e., with increasing BET surface area or surface-to-volume ratio.

Bubble coalescence was quantified by analyzing sequences of x-ray images using the software AXIM (see Ref. 35). Bubble coalescence in foams made by PIF of precursors obtained by pressing powders of different particle sizes as well as in standard PM foams blown with TiH_2 was quantified in the liquid state by tracking the cumulative cell wall ruptures after full expansion. The sum of the cell wall rupture events shown in Fig. 7 shows that the coalescence rate in PIF-processed foams is about three times lower than in a comparable standard PM foam of similar density made from as-received powders under the same conditions but containing 0.5 wt.% TiH_2 acting as a blowing agent.

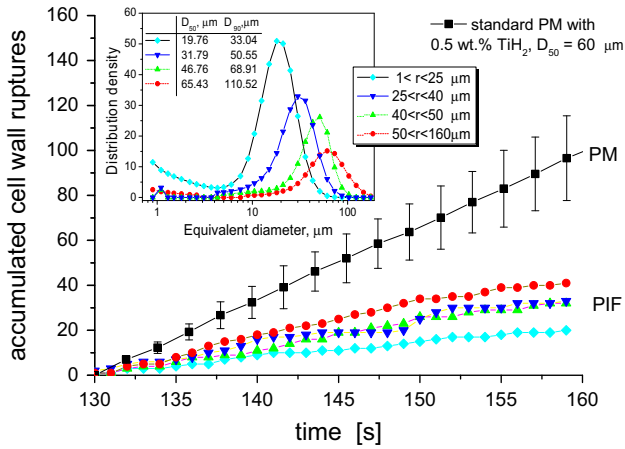


Fig. 7. Accumulated coalescence events (film ruptures) during 30 s of holding in fully expanded Al foams blown with 0.5 wt.% TiH₂ and Al foams made by PIF ($p_0 = 5$ bar), the latter for different powder particle sizes ($D_{50} = 20, 32, 47,$ and $65 \mu\text{m}$). Inset: Particle size distribution for sieved powders and mean particle sizes D_{50} and D_{90} .

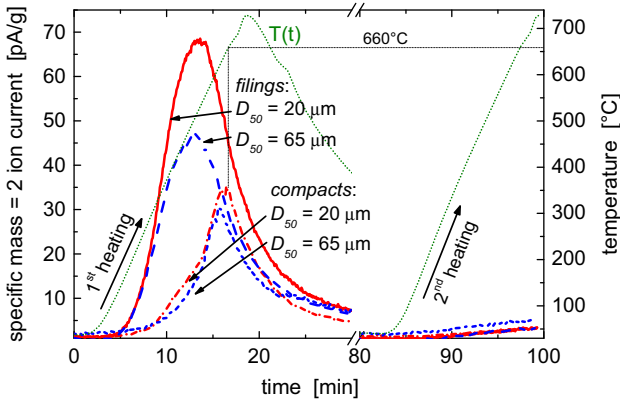


Fig. 8. Mass = 2 ion current representing the hydrogen gas release (or loss) from Al powder compacts and loose filings thereof. Fine ($D_{50} = 20 \mu\text{m}$) and coarse powder ($D_{50} = 65 \mu\text{m}$) is used. Heating cycles are carried out under flowing Ar at a heating rate of 5 K/min. The first cycle and part of the second one are shown in this figure.

Gas Release Analysis

The release of hydrogen gas from an Al99.7 powder compact and from the corresponding loose filings as a function of temperature is given in Fig. 8 for constant heating at 5 K/min under flowing Ar. The gas release analysis showed that hydrogen is the only gas that provides sufficient volume to foam the samples. A comparison between subsequent heating cycles reveals that most of the hydrogen gas is released during the first heating cycle and below the melting point of Al (660°C) and very little in the second or further cycles. A comparison between samples made from finer ($D_{50} \approx 20 \mu\text{m}$) and coarser powders ($D_{50} \approx 65 \mu\text{m}$) shows that the smaller the powder size, the more hydrogen can be detected.

DISCUSSION

For foaming a liquid metal, two main conditions have to be satisfied. First, the films between

adjacent bubbles need to be stabilized either by the added ceramic particles or by the oxides contained in the metal powders used as base material.³⁶ Second, a gas source is required that releases sufficient amounts of gas in the right temperature range. As PIF is a powder-based process, stabilization is provided by the same mechanism known from the traditional PM process.^{25–27}

During heating of a powder compact made without blowing agent at ambient pressure, the gas produced through desorption from the powder surfaces or contained in porosity, defects, or cavities in the precursor does not lead to a notable expansion, probably due to the small gas volume and losses to the surroundings while the material is still solid. During solidification, the solubility of hydrogen decreases, resulting in a small expansion due to gas nucleation.³⁷

In the following, we estimate how much gas can be expected from the most likely gas sources and compare the figures with the amount of gas that can be produced by a blowing agent.

Gas Sources

The results presented show that foaming of hot-compacted metallic powders without blowing agent is possible by PIF. This indicates the presence of gas sources in the precursors that act as “intrinsic” blowing agents and provide sufficient gas to nucleate inside the compacted precursors during melting and then to expand to a considerable volume when the overpressure is released. Such gas could either be present in the compacted metallic powders or could be gas that has been entrapped during precursor compaction. It is certain that use of powders is essential because bulk samples of cast Al or Al alloys cannot be foamed by gas release. Cast Al samples melted under 1 bar show just a small expansion of $A_{f,\text{max}}/A_0 = 1.06 \pm 0.03$ corresponding to the thermal expansion.

We consider Al alloy precursor samples of volume V_0 . For the reference samples containing 0.5 wt.% TiH₂, the theoretical volume V_{g0} of hydrogen present in the blowing agent at 1 bar pressure allows us to assess the gas volume needed for foaming. The concentration of hydrogen gas in the precursor is:

$$c_{\text{H}}(\text{Al}_{\text{pr}}) = c_{\text{TiH}_2}(\text{Al}_{\text{pr}}) \times c_{\text{H}}(\text{TiH}_2) = 2 \times 10^{-4} \quad (3)$$

$c_{\text{H}}(\text{TiH}_2) = 0.04$ and $c_{\text{TiH}_2}(\text{Al}_{\text{pr}}) = 0.005$ are the relative concentration of hydrogen in TiH₂ and of TiH₂ in the Al precursor, respectively. With $\rho_{\text{pr}} \approx \rho_{\text{Al}} = 2.7 \text{ g/cm}^3$, the corresponding amount of hydrogen in the precursor is 0.54 mg/cm^3 . If this gas is treated as ideal, then its volume at 660°C is $V_{g0}(660^\circ\text{C}) = 0.54/2 \times 10^{-3} \times 22.4 \times 10^3 \times (933/273) \times V_0 \approx 20 \times V_0$. If all this hydrogen gas contributed to foam formation ($V_f = (20 \times V_0) + V_0$), then a relative volume expansion factor of $V_f/V_0 \approx 21$ would be expected. Usually, foam expansion

sion for free foaming is in the range of $V_f/V_0 \approx 5-7$ ^{12,14} which implies that at most 1/5 to 1/4 of the hydrogen gas contained in the blowing agent contributes to foam expansion and that a large part of the hydrogen must be still bound in TiH_2 , e.g., as another TiH_x -phase in the matrix^{18,19,38} or is lost during the process by (I) dissolution in the melt, (II) out-diffusion from the foam,³⁹ or (III) by escaping to the surrounding through cracks in the precursor or rupture of outer bubbles.^{7,38}

For PIF, the most likely gas sources include:

1. Gas dissolved in the metal
2. Entrapped gas and porosity within the powder particles
3. Gas adsorbed to the metal powder surfaces

Gas Dissolved in the Metal

Hydrogen is the only gas that can be dissolved in Al in considerable volumes,⁴⁰ although its solubility is still lower than in many other metals.²³ In PIF, the gas pressure is released at a constant temperature slightly above the melting temperature³⁷ and hydrogen precipitation during solidification cannot occur. However, gas can precipitate during pressure release because, according to Sievert's law, the solubility is given by the external pressure:

$$c_H \sim p^{1/2} \quad (4)$$

In our case, reducing pressure from $p_0 = 9$ bar to $p_1 = 1$ bar will reduce solubility to 1/3 of the high-pressure value because

$$c_H(p_1)/c_H(p_0) \sim (p_1/p_0)^{1/2} = 1/3 \quad (5)$$

The hydrogen solubility in liquid Al at $T_m(\text{Al}) = 660^\circ\text{C}$ is $S_H(\text{Al}) = 0.69 \text{ cm}^3/100 \text{ g Al}$.^{23,41-43} Therefore, the maximal hydrogen volume that can be liberated from an Al precursor of volume of V_0 is $V_{gI}(660^\circ\text{C}, 9 \text{ bar}) = V_0 \times 2.7 \times 2/3 \times 0.69 \times 10^{-2} = V_0 \times 3.73 \times 10^{-2}$, which is too low for foaming.

The gas volume obtained is far below the volume needed for foaming. Recent work showed that hydrogen outdiffusion through a metal foam skin depends on the surrounding atmosphere.³⁹ PIF under argon and with different waiting times (10 s and 100 s) between melting and pressure release showed no notable variation in expansion. We can conclude that the hydrogen dissolved in the melt cannot play a key role for foaming.

Entrapped Gas and Internal Porosity of Metal Powders

The density of our compacted powder precursors is $\rho \approx 99\%$ of the bulk density or higher, implying that all the gas entrapped during compaction, e.g.,

in bifilms as known from castings,⁴⁴ together with the internal porosity of the Al powders and pores at the boundaries of former powder particles give rise to a total porosity of $P \leq 1\%$ in the precursor. If the internal pressure in such pores is 1 bar, this corresponds to a maximal volume of $V_{gII}(20^\circ\text{C}) \leq V_0 \times 10^{-2}$ and $V_{gII}(660^\circ\text{C}) \leq V_0 \times 3.18 \times 10^{-2}$, which is also too low for foaming.

This gas volume would be much higher if the porosity contained gas under elevated pressure. Theoretically, the pressing die could contain up to three times more air volume than powder volume, and this gas would be entrapped tightly under high pressure inside the 1% porosity of the precursor. In this case, V_{gII} at 1 bar pressure could range up to $\approx 3 V_0$. However, the gas actually released during foaming should depend on the gas pressure during pressing. We found that pressing the powders under a defined gas pressure of 2 bar yielded the same results as pressing under 1 bar pressure. Furthermore, precursors compacted under very low pressure, namely 10^{-2} bar, showed a homogeneous pore size distribution and a notably increased expansion compared with the ones compacted under 1 bar; see Fig. 6 and "Influence of Precursor Preparation" section, which can be explained by the better sintering of the grains, as it is known for vacuum pressing of Al-based foamable precursors.⁷ These experiments disprove that entrapped gas is a dominant gas source for foam expansion.

Diffusion of hydrogen gas into the precursor through its surfaces due to the increased surrounding overpressure during heating is possible, but the amount of hydrogen dissolved cannot be more than the solubility limit. Considering 1% porosity in the precursor, V_{gII} will be again in the range of $\approx V_0 \times 10^{-2}$ but at a maximum pressure of p_0 , providing a maximum gas volume of just $V_{gII} \approx V_0 \times 10^{-1}$ at 1 bar. Such indiffusion of gas into a precursor should allow PIF also for a cast Al precursor, but this was experimentally disproved (see "Influence of Precursor Preparation" section). Using overpressure during melting of the precursor, even if it exhibited fully open porosity like is the case in a cold compacted precursor, was not amenable to pressure-induced expansion (see "Influence of Precursor Preparation" section). Porosity and entrapped gas can therefore not be the principle gas sources for PIF.

Gas Adsorbed to the Metal Powder Surfaces

As the surface-to-volume ratio of the initial metal powder is high compared with a bulk of the same mass, atomic or molecular adsorbates, such as H_2 , O_2 , N_2 , CO , CO_2 , H_2O , hydroxides, and hydrocarbons, are present^{45,46} and could contribute to gas generation. We can distinguish between physisorption with a coverage of $\theta = 1$ (i.e., one monolayer of adsorbate) and chemisorption with $\theta \geq 1$.⁴⁷ The kinetics of adsorption are ruled by the sticking prob-

Table I. Theoretical hydrogen volumes in an aluminum foam made from an Al99.7 precursor of volume V_0 compared to the real gas volume in a solidified foam

Real gas Volume in foam	Theoretical hydrogen volumes generated in different ways			
	0.5 wt.% TiH ₂	Dissolved hydrogen	Entrapped air	Adsorbed gas
V_g (660°C) $4-6 \times V_0$	V_{g0} (660°C) $20 \times V_0$	V_{gI} (660°C) $3.7 \times 10^{-2} \times V_0$	V_{gII} (660°C) $3.2 \times 10^{-2} \times V_0$	V_{gIII} (660°C) $10.3 \times V_0$

Four different hydrogen sources are considered.

abilities of gases on the surfaces of solids.⁴⁸ During exposure of Al powder to air oxidation will proceed until the limit set by the theory of Cabrera and Mott.⁴⁹ This natural oxide layer is ≈ 2 nm thick^{50,51} and shows a strong tendency for hydration, especially when exposed to humid environments. Al powders also pick up atomic H in solution from the hydrated layer during thermal treatments such as hot compaction.⁵² Hydration of the oxide layer at the powder surface leads to both physically adsorbed and chemically bonded water as hydroxide.^{53,54} During heating, H₂O is desorbed and the hydroxide decomposes producing boehmite and more water.⁵⁵ The water production continues above 310°C, and it can oxidize Al and form hydrogen gas. Between 400°C and 500°C, hydrogen production peaks. At about 500°C, most of the water has been released.⁵⁵ For example, it was found that the hydrogen contents in Al-based powder are 700 (air atomized) or 566 (nitrogen atomized) times higher than the maximum solubility of hydrogen in solid aluminum.^{53,56}

We can estimate that our air-atomized Al powder with $D_{50} = 38 \mu\text{m}$ has a typical surface of $\approx 0.3 \pm 0.05 \text{ m}^2/\text{g}$.^{51,53} The total powder surface S_p in an Al precursor of volume V_0 therefore is $S_p = V_0 \times 8.1 \times 10^3 \text{ cm}^{-1}$. The water molecule density of a monolayer adsorbed to aluminum is $\approx 10^{15} \text{ mol}/\text{cm}^2$, the total amount of water molecules $\approx 0.03 \mu\text{g}/\text{cm}^2$.⁵⁷⁻⁵⁹ For a single monolayer of water covering the Al powder grains, the total number of water molecules in a precursor will be $N_{\text{H}_2\text{O}} \approx V_0 \times 8.1 \times 10^{18} \text{ cm}^{-3}$. For Al powder surfaces, an adsorption of $n_{\text{mono}} \approx 10$ monolayers was found,^{55,59} corresponding to a total mass of adsorbed water of $\approx V_0 \times 0.3 \mu\text{g}/\text{cm}^2$. The resulting gas volume V_{gII} can be calculated using Loschmidt's constant $N_L = 2.687 \times 10^{19} \text{ cm}^{-3}$ to $V_{gIII} (0^\circ\text{C}) = n_{\text{mono}} \times N_{\text{H}_2\text{O}}/N_L \approx V_0 \times 3.015$ and $V_{gIII} (660^\circ\text{C}) \approx V_0 \times 10.3$. This gas volume can indeed result in a considerable expansion, which indicates that the adsorbates are the main gas source for PIF. Table I compares all possible gas sources.

Other Aspects of Gas Generation

Heating blowing agent free powder compacts under constant ambient pressure also leads to gas

nucleation of the adsorbed gas and a small expansion (see Figs. 2 and 4) in the range of $A_f/A_0 \approx 1.3 \pm 0.1$ for AlSi7 and $A_f/A_0 \approx 1.4 \pm 0.1$ for pure Al, which is far beyond pure thermal expansion in the solid and during melting, as it is observed in cast Al where $A_f/A_0 \approx 1.06 \pm 0.03$.

Because the samples are melted under overpressure ($p_0 > p_1$) in PIF, gas losses are reduced during the heating and the foaming phase in comparison to foaming with blowing agent following the standard PM route under 1 bar. This means that the total gas volume required inside the precursor should be considerably less than the volume V_g produced during conventional blowing-agent-assisted foaming. At the foaming temperature, the adsorbates are fully dissociated and contribute to expansion, whereas with blowing agent, part of the hydrogen does not dissociate and contribute to foaming, but rather it remains inside the Ti lattice as a TiH_x phase.¹⁸

Applying a low pressure of $p_0 = 10^{-2}$ bar during the heating stage of a PIF experiment until the precursor was melted, followed by a pressure increase up to $p_0 = 9$ bar and a subsequent pressure release to $p_1 = 1$ bar did not initiate foaming (see "Influence of Pressure" section). This implies that the foaming gas was not trapped in the sample, but it was lost during the heating stage below the foaming temperature.

If surface adsorbates are responsible for PIF, the surface-to-volume ratio of the powder should play a key role because the effective surface area S_p is larger for finer powders. Indeed (see Fig. 6), the expansion of samples made from powders with larger surface areas is clearly higher. This corroborates the idea that adsorbates are the principle gas source for PIF. However, the increase of foam expansion with smaller powder particle size is below the corresponding increase of the powder surface area. One reason for this could be the different compaction properties of powders with different sizes and size distributions. The various contributions that lead to foam expansion are possibly additive, but according to Table I, only adsorbates are capable of generating enough gas to explain the large expansion during PIF.

Process Parameters

The choice of parameters applied for producing PIF precursors was based on the procedures known from pressing precursors containing blowing agents. Pressing has to create a metallic bonding between Al powder particles in both cases to obtain a gas-tight metallic matrix. Cold compaction of Al powders, although feasible,^{60,61} often does not lead to well foamable precursors, which is why uniaxial hot compaction was used.

PIF does not work under a soft vacuum. If a starting pressure of, e.g., $p_0 = 10^{-1}$ bar is selected, then the gas forming in the precursor forms unstable bubbles that coalesce immediately to larger bubbles that ascend to the surface due to buoyancy and rupture there. The gas is lost to the surroundings. Further gas release by pulling a stronger vacuum, for instance to $p_1 = 10^{-3}$ bar, does not induce any foaming. This result is similar to experiments with blowing agents under low pressures¹⁴ but is distinct from the case of Mg slurries,²² where Mg foams could be produced by pulling a vacuum. The reason for this can be the increased self-stabilization in this special case of a Mg alloy melt heavily loaded with oxides.

Foaming time was found to have little influence on the expansion or coalescence for the parameter range investigated ($t_f = 5$ s, 25 s, and 60 s). This indicates that the internal pressure follows the outer pressure, and little gas is lost to the surroundings after melting as shown in Fig. 8.

Foam Expansion

The total foam volume can be expressed as

$$V_f(t) = V_0 + V_g(p) \quad (6)$$

And, according to the ideal gas law and at constant temperature, we obtain

$$V_g(p_1)/V_g(p_0) = p_0/p_1 \quad (7)$$

The expansion under pressure p_0 described in “[Influence of Pressure](#)” section corresponds to the gas volume, which is responsible for foaming during pressure release. For example, the release from $p_0 = 9$ bar to $p_1 = 1$ bar in Fig. 4 results in a relative cross-sectional expansion of $A_f/A_0 = 1.9$ compared to the original precursor, which roughly corresponds to $V_f/V_0 = 2.6$ according to Eq. 2. For a pressure release from, e.g., $p_0 = 2$ bar to $p_1 = 1$ bar, the gas volume in the foam $V_g(p_0)$ should double according to Eq. 7 at constant T to $V_g(p_1)$ assuming no losses.

The pressure dependence of the cross-sectional expansion can be deduced from Eqs. 2, 6, and 7:

$$\frac{A_f(p_1)}{A_0} = \left(\frac{p_0}{p_1} \frac{V_g(p_0)}{V_0} + 1 \right)^{2/3} \quad (8)$$

For the experimental values $V_0 = 1 \text{ cm}^3$ and $A_f(p_0)/A_0 = 1.3$ (see Fig. 4), and assuming then $V_f = 1.5 \text{ cm}^3$ with Eq. 2 and $V_g(p_0) = 0.5 \text{ cm}^3$ with Eq. 6, the theoretical cross-sectional expansion can be written as:

$$\frac{A_f(p_1)}{A_0} = (1 + 0.5p_0)^{2/3} \quad (9)$$

Figure 4 compares the experimental and theoretical values of the area expansion. The measured expansion increases with p_0 but slower than theoretically expected. This is caused by other effects that have to be considered, such as gas losses due to bubble ruptures at the surface or due to gas diffusion through the foam surfaces into the surroundings leading to foam collapse, or by intrinsic instabilities of the foam structure at large expansions. In Fig. 8, for example, the hydrogen release from compacts decreases after melting (660°C after 16.5 min) but does not go to zero.

From Laplace’s law, we know that gas nucleation will take place when the critical radius $R_c = 2\sigma/p_L$ is reached, where σ is the liquid–gas interfacial energy and p_L is the Laplace pressure of the bubble. If we consider $p_L \approx p_0$ in a diffusion equilibrium with the surroundings, the critical bubble radii during nucleation should become smaller with increasing p_0 . This leads to a higher chance for gas to nucleate instead of diffusing to existing nuclei. Thus, the number of nucleation centers also increases with increasing p_0 , similar to what was found in samples foamed with TiH_2 .¹⁴

Figure 5 shows an Al99.7 PIF-foam with an increased expansion of $A_{f,\text{max}}/A_0 \approx 3$ for $p_0 = 5$ bar and $p_1 = 1$ bar with round and uniformly distributed pores. This improvement was achieved by hot pressing the sample under the low pressure of $\approx 10^{-2}$ bar in order to enhance powder compaction and to avoid oxidation of the fresh powder surfaces exposed during hot compaction.^{55,62} As a result, the gas available for subsequent foaming is better trapped in the metal matrix. In vacuum hot-compacted compacts, fewer cracks form during heating and gas loss is reduced;⁷ thus, foam expansion improves.

Foam Stability

Stabilization of the liquid films in expanding foams is caused by the oxide filaments and networks originating from the oxidized surfaces of the metallic powders used. It is reasonable to assume that the stabilization mechanism is the same for PIF and foaming with a blowing agent. TiH_2 other than carbonates does not produce a gas that can lead to particle formation,^{26,27} and the remnants of TiH_2 decomposition are not distributed densely enough to stabilize the films.

To study the stability of metallic foams in the liquid state quantitatively, we analyzed bubble coalescence throughout foaming. In PIF foams, coalescence was found to be just $\approx 1/3$ of the value in similar foams blown with TiH_2 (see Fig. 7), although the number of bubbles is increased in PIF due to the high nucleation rate, which would rather induce an increased rupture probability. Moreover, no collapse after expansion was found for any of the PIF samples. Bubble expansion during PIF takes place under conditions of a uniformly distributed pressure field, with the only gradient being between the foam interior and the surroundings. After foaming is induced by pressure release, no gas source is active anymore and no inter-bubble pressure gradients develop. This is different when TiH_2 drives expansion because the temperature-sensitive blowing agent with its wide distribution of particle sizes can generate pressure gradients that overstretch individual films and trigger rupture, which is why the observed coalescence effect is much stronger.

Our experiments under microgravity showed that TiH_2 plays a more important role than gravity-induced drainage in causing film rupture in Al-based PM foams.^{63,64} An increased cell wall stability effect was also found for Zn-based foams blown with an intrinsic gas source.⁴⁰

Advantages of PIF Versus Blowing Agent Foaming

PIF could gain industrial relevance. The costs for the blowing agent powder, its pretreatment, and powder mixing can be avoided. Process temperature control is less critical in PIF than in the cases where blowing agents are used.^{14,33} For foaming net-shape components, a gas-tight mold equipped with a gas release valve can be used. On the other hand, the additional pressure control required would reduce the cost benefit.

Foaming times can be very short ($t_f \approx 10\text{--}15$ s) compared with the times usually needed to expand foams with TiH_2 (usually 30–300 s). Such long periods of expansion increase stochastic cell wall rupture events and lead to a coarser pore structure. The heating time is similar for both methods. A more uniform pore nucleation due to the overpressure applied and the possibility of precisely controlling expansion, density, and pore size by adjusting $p_1\text{--}p_0$ represents additional benefits of PIF.³⁰

The foams made by PIF are more stable in the liquid state than the ones blown by TiH_2 , making the process window wider. This is proven by the clear reduction of the coalescence rate in the liquid state, as demonstrated in Fig. 7. PIF foams are also very uniform in pore size (see Fig. 3).

From the scientific viewpoint, PIF allows for an easier analysis of the foaming conditions of metals, especially its temperature dependence, because complications in analysis due to the extreme tem-

perature sensitivity of gas generation from a blowing agent are not present.^{37,40,65}

SUMMARY

PIF is a foaming method based on compacted metal powders. Other than the traditional foaming methods, it does not require additional blowing agents. When melting hot-compacted Al powders under gas overpressure and then releasing the pressure, the gas contained in the sample expands in area by $A_f/A_0 \approx 3$, corresponding to a volume expansion of $V_f/V_0 \approx 5.2$, which is comparable to foaming with a blowing agent. The high pressure during melting hinders gas losses during heating and induces nucleation of a multitude of uniformly distributed bubbles, which evolve into a uniform expanded foam. Cross-sectional expansion increases when the initial overpressure p_0 is higher. The coalescence rate during foam expansion triggered by pressure release was found to be three times lower than when foaming was driven by TiH_2 . Different possible gas sources were analyzed and their contributions estimated. Adsorbates were identified as the main gas source for PIF. PIF could become an industrially relevant foaming method because neither blowing agents nor precise temperature control are needed to produce high-quality foams. In addition, the foam density and foaming time are easily adjustable.

ACKNOWLEDGEMENTS

Funding by the European Space Agency ESA (Project $\mu\text{G-Foam}$, AO-99-075) is gratefully acknowledged.

REFERENCES

1. J. Banhart, *JOM* 52, 22 (2000).
2. C.S. Shim, N.R. Yun, I.H. Yu, and D.Y. Byun, *Porous Metals and Metallic Foams: Metfoam*, ed. B.-Y. Hur (Busan: Gyeongsang National University, 2012), p. 501.
3. J. Banhart and H.-W. Seeliger, *Adv. Eng. Mater.* 14, 1082 (2012).
4. R. Neugebauer and T. Hipke, *Adv. Eng. Mater.* 8, 858 (2006).
5. J. Banhart, *Adv. Eng. Mater.* 8, 781 (2006).
6. P. Schäffler, G. Hanko, H. Mitterer, and P. Zach, *Porous Metals and Metallic Foams: Metfoam*, ed. L.P. Lefebvre, J. Banhart, and D.C. Dunand (Kyoto: The Japan Institute of Metals, 2008), p. 7.
7. C. Jiménez, F. Garcia-Moreno, M. Mukherjee, O. Goerke, and J. Banhart, *Scripta Mater.* 61, 552 (2009).
8. A. Rack, H.M. Helwig, A. Bütow, A. Rueda, B. Matijasević-Lux, L. Helfen, J. Goebbels, and J. Banhart, *Acta Mater.* 57, 4809 (2009).
9. J. Banhart, D. Bellmann, and H. Clemens, *Acta Mater.* 49, 3409 (2001).
10. B. Matijasevic-Lux, J. Banhart, S. Fiechter, O. Görke, and N. Wanderka, *Acta Mater.* 54, 1887 (2006).
11. F. von Zeppelin, M. Hirscher, H. Stanzick, and J. Banhart, *Compos. Sci. Technol.* 63, 2293 (2003).
12. I. Duarte and J. Banhart, *Acta Mater.* 48, 2349 (2000).
13. F. Simancik, K. Behulova, and L. Bors, *Cellular Metals and Metal Foaming Technology: Metfoam*, ed. J. Banhart, M.F. Ashby, and N.A. Fleck (Bremen: MIT Publishing, 2001), p. 89.

14. F. Garcia-Moreno, N. Babcsan, and J. Banhart, *Colloids Surf. A* 263, 290 (2005).
15. F. Garcia-Moreno, J. Banhart, M. Haesche, K. Vignodhar, and J. Weise, *Cellular Metals for Structural and Functional Applications. Cellular Metals for Structural and Functional Applications: CellMet*, ed. G. Stephani and B. Kieback (Dresden: Fraunhofer IRB Verlag, 2005), p. 244.
16. A. Kennedy and V. Lopez, *Mater. Sci. Eng. A* 357, 258 (2003).
17. V.A. Lavrenko, V.Z. Shemet, L.A. Petrov, O.A. Teplov, and S.K. Dolukhanyan, *Oxid. Met.* 33, 177 (1990).
18. C. Jiménez, F. Garcia-Moreno, B. Pfretzschner, M. Klaus, M. Wollgarten, I. Zizak, G. Schumacher, M. Tovar, and J. Banhart, *Acta Mater.* 59, 6318 (2011).
19. C. Jiménez, F. Garcia-Moreno, A. Rack, R. Tucoulou, M. Klaus, B. Pfretzschner, T. Rack, P. Cloetens, and J. Banhart, *Scripta Mater.* 66, 757 (2012).
20. M. Mukherjee, F. Garcia-Moreno and J. Banhart, *Scripta Mater.* 63, 235 (2010).
21. U. Ramamurty and A. Paul, *Acta Mater.* 52, 869 (2004).
22. K. Renger and H. Kaufmann, *Adv. Eng. Mater.* 7, 117 (2005).
23. D.E.J. Talbot, *Int. Metall. Rev.* 20, 166 (1975).
24. H.E. Friedrich and B.L. Mordike, *Magnesium Technology: Metallurgy, Design Data, Applications* (New York: Springer, 2006).
25. S. Asavavisithchai and A.R. Kennedy, *J. Colloid Interface Sci.* 297, 715 (2006).
26. A. Dudka, F. Garcia-Moreno, N. Wanderka, and J. Banhart, *Acta Mater.* 56, 3990 (2008).
27. C. Körner, M. Arnold, and R.F. Singer, *Mater. Sci. Eng. A* 396, 28 (2005).
28. G.S. Vinod Kumar, M. Mukherjee, F. Garcia-Moreno, and J. Banhart, *Metall. Mater. Trans. A* 44, 419 (2013).
29. F. Garcia-Moreno and J. Banhart, *Colloids Surf. A* 309, 264 (2007).
30. F. Garcia-Moreno and J. Banhart, European patent EP 1 915 226 B1 (2007), p. 10.
31. A. Ünal, *Mater. Sci. Technol.* 3, 1029 (1987).
32. F. Garcia-Moreno, N. Babcsán, and J. Banhart, *Metfoam*, ed. N.K.H. Nakajima (Kyoto: The Japan Institute of Metals, 2006), p. 129.
33. F. Garcia-Moreno, M. Fromme, and J. Banhart, *Adv. Eng. Mater.* 6, 416 (2004).
34. M.A. Rodriguez-Perez, E. Solorzano, J.A. De Saja, and F. Garcia-Moreno, *Porous Metals and Metallic Foams: Metfoam*, ed. L.P. Lefebvre, J. Banhart, and D.C. Dunand (Montreal: DEStech, 2008), p. 75.
35. F. Garcia-Moreno, E. Solorzano, and J. Banhart, *Soft Matter* 7, 9216 (2011).
36. A. Haibel, A. Rack, and J. Banhart, *Appl. Phys. Lett.* 89, 154102 (2006).
37. M. Mukherjee, F. Garcia-Moreno, and J. Banhart, *Acta Mater.* 58, 6358 (2010).
38. C. Jiménez, F. Garcia-Moreno, B. Pfretzschner, P.H. Kamm, T.R. Neu, M. Klaus, C. Genzel, A. Hilger, I. Manke, and J. Banhart, *Adv. Eng. Mater.* 15, 141 (2013).
39. M. Mukherjee, F. Garcia-Moreno, and J. Banhart, *Metall. Mater. Trans. B* 41, 500 (2010).
40. M. Mukherjee, F. Garcia-Moreno, C. Jiménez, and J. Banhart, *Adv. Eng. Mater.* 12, 472 (2010).
41. C. Qiu, G.B. Olson, S.M. Opalka, and D.L. Anton, *J.P.E.D.* 25, 520 (2004).
42. H. Nakajima, T. Ikeda, and S.K. Hyun, *Adv. Eng. Mater.* 6, 377 (2004).
43. P. Lutze and J. Ruge, *Metall* 8, 741 (1990).
44. J.T. Staley, M. Tiryakioglu, and J. Campbell, *Mater. Sci. Eng. A* 460–461, 324 (2007).
45. S. Khoobiar, J.L. Carter, and P.J. Lucchesi, *J. Phys. Chem.* 72, 1682 (1968).
46. F.o. Rouquerol, *Adsorption by Powders and Porous Solids: Principles, Methodology and Applications* (Waltham, MA: Academic Press, 1999).
47. D.M. Ruthven, *Principles of Adsorption and Adsorption Processes* (New York: Wiley, 1984).
48. P. Kisliuk, *J. Phys. Chem. Solids* 3, 95 (1957).
49. N. Cabrera and N.F. Mott, *Rep. Prog. Phys.* 12, 163 (1949).
50. A.V. Krajinikov, M. Gastel, H.M. Ortner, and V.V. Likutin, *Appl. Surf. Sci.* 191, 26 (2002).
51. L. Kowalski, B.M. Korevaar, and J. Duszczkyk, *J. Mater. Sci.* 27, 2770 (1992).
52. G. Staniek and K. Wefers, *Aluminium* 67, 160 (1991).
53. J.L. Estrada, J. Duszczkyk, and B.M. Korevaar, *J. Mater. Sci.* 26, 1431 (1991).
54. S. Meng, E. Wang, and S. Gao, *Phys. Rev. B: Condens. Matter* 69, 155406 (2004).
55. A. Nylund and I. Olefjord, *Mater. Sci. Eng. A* 134, 1225 (1991).
56. J. Zhou, J. Duszczkyk, and B.M. Korevaar, *J. Mater. Sci.* 26, 3292 (1991).
57. J.R. Chen, G.Y. Hsiung, Y.J. Hsu, S.H. Chang, C.H. Chen, W.S. Lee, J.Y. Ku, C.K. Chan, L.W. Joung, and W.T. Chou, *Appl. Surf. Sci.* 169, 679 (2001).
58. W.H. Krueger and S.R. Pollack, *Surf. Sci.* 30, 280 (1972).
59. L. Volpe, *Key Eng. Mater.* 20–28, 4091 (1991).
60. L. Bonaccorsi, E. Proverbio, and N. Raffaele, *J. Mater. Sci.* 45, 1514 (2010).
61. A.R. Kennedy, *Powder Metall.* 45, 75 (2002).
62. G.B. Schaffer, B.J. Hall, S.J. Bonner, S.H. Huo, and T.B. Sercombe, *Acta Mater.* 54, 131 (2005).
63. F. Garcia-Moreno, M. Mukherjee, C. Jiménez, A. Rack, and J. Banhart, *Metals* 2, 10 (2011).
64. F. Garcia-Moreno, M. Mukherjee, C. Jiménez, and J. Banhart, *Trans. Indian Inst. Met.* 62, 451 (2009).
65. C. Jiménez, F. Garcia-Moreno, J. Banhart, and G. Zehl, *Porous Metals and Metallic Foams: Metfoam*, ed. L.P. Lefebvre, J. Banhart, and D. Dunand (Montréal: DEStech, 2008), p. 59.